

Azimuthal Correlations in electroproduction



Rahul Basu

The Institute of Mathematical Sciences
Taramani, Chennai 600 113
India

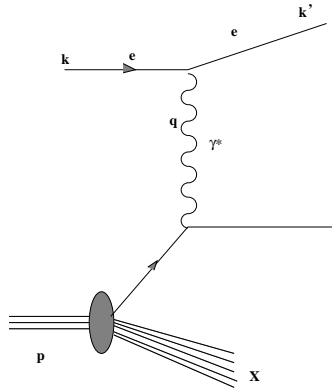
<http://www.imsc.res.in/~rahul>

Deep Inelastic Scattering at HERA

$e^+ - P$ collider machine which reached very small values of Bjorken x :

$$e(k) + P(p) \rightarrow e(k') + X$$

The following kinematic variables completely describe the process:



$$s = (k + p)^2 \simeq 4E_e E_p$$

$$Q^2 = -q^2 \simeq 2E_e E_{e'} (1 + \cos\theta)$$

$$y = \frac{p \cdot q}{p \cdot k} \simeq 1 - \frac{E_{e'}}{2E_e} (1 - \cos\theta)$$

$$x = \frac{Q^2}{2p \cdot q} \simeq \frac{Q^2}{ys}$$

$$W = (q + p)^2 \simeq -Q^2 + ys$$

HERA has provided an unprecedented view into the structure of the proton at low x and large Q^2 .

Measurement of F_2

The Born cross section for single photon exchange in DIS :

$$\frac{d^2\sigma}{dx dQ^2} = \frac{2\pi\alpha^2}{Q^2 x} \left[2(1-y) + \frac{y^2}{1+R} \right] F_2(x, Q^2)$$

R is the photoproduction cross section ratio for longitudinal and transverse polarised photon,

$$R = \sigma_L / \sigma_T$$

Physics limitations in F_2 measurement

- Rise in F_2 as a function of x (for all $Q^2 > 1\text{GeV}^2$) is explained very well by standard perturbative QCD (**DGLAP equations**) - an evolution in Q^2 carried out by summing over $\ln Q^2$ terms.

Physics limitations in F_2 measurement

- Rise in F_2 as a function of x (for all $Q^2 > 1\text{GeV}^2$) is explained very well by standard perturbative QCD (**DGLAP equations**) - an evolution in Q^2 carried out by summing over $\ln Q^2$ terms.
- The same rise is also predicted satisfactorily within experimental errors by the BFKL equation which sums $\ln(1/x)$ terms.

Physics limitations in F_2 measurement

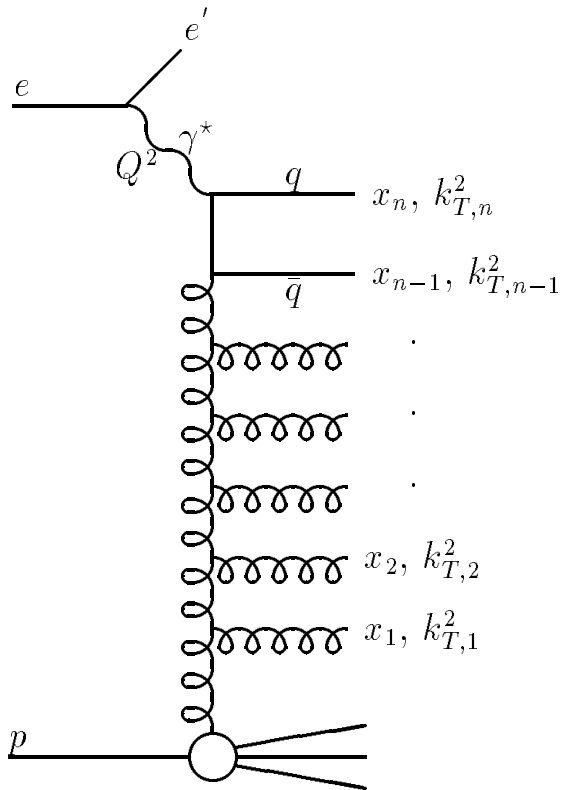
- Rise in F_2 as a function of x (for all $Q^2 > 1\text{GeV}^2$) is explained very well by standard perturbative QCD (**DGLAP equations**) - an evolution in Q^2 carried out by summing over **$\ln Q^2$** terms.
- The same rise is also predicted satisfactorily within experimental errors by the BFKL equation which sums **$\ln(1/x)$** terms.
- So how does one distinguish these different **resummation** schemes?

Forward Jets and Single Particle Production

The cross section for forward jet production in DIS was suggested by Mueller (Mueller 1991, Mueller, Navelet 1991) as a means of distinguishing these different **resummation** schemes.

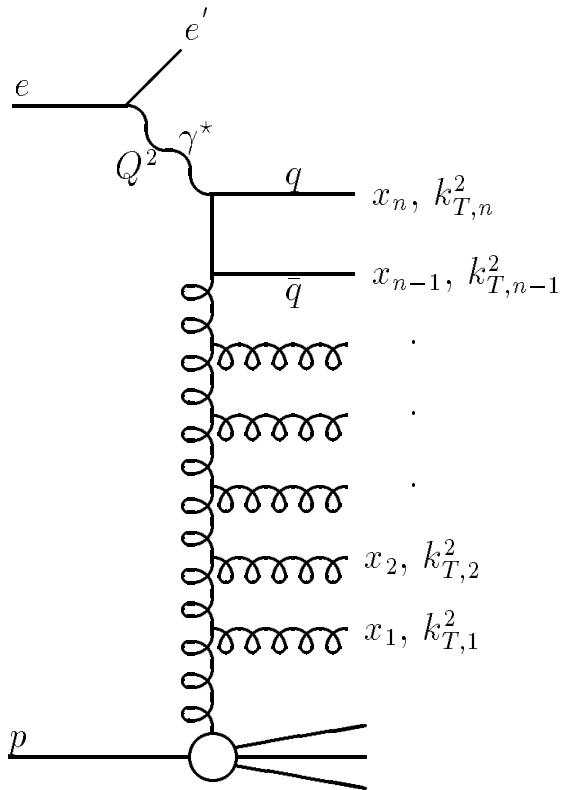
Forward Jets and Single Particle Production

The cross section for forward jet production in DIS was suggested by Mueller (Mueller 1991, Mueller, Navelet 1991) as a means of distinguishing these different **resummation** schemes.



Forward Jets and Single Particle Production

The cross section for forward jet production in DIS was suggested by Mueller (Mueller 1991, Mueller, Navelet 1991) as a means of distinguishing these different **resummation** schemes.

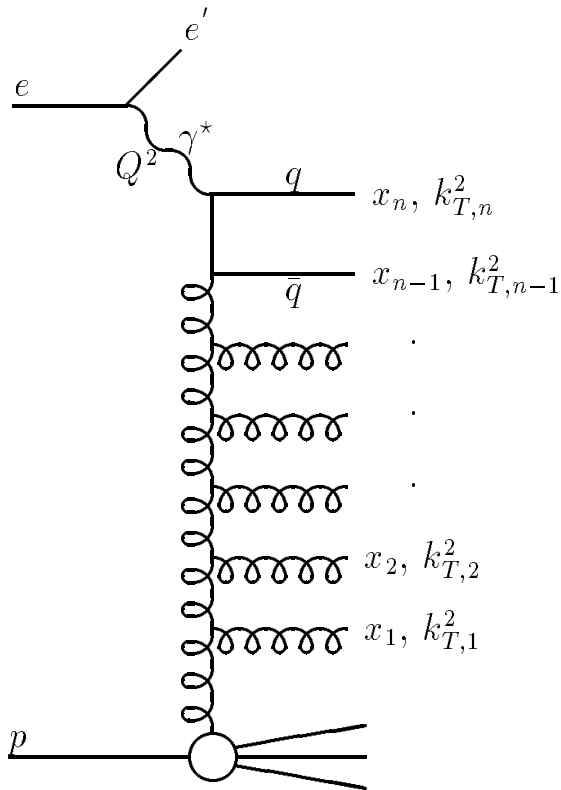


DGLAP and BFKL predict different ordering of the transverse momenta $k_{T,i}$ along the parton cascade developing in DIS jet production. DGLAP predicts strong $k_{T,i}$ ordering ($Q^2 = k_{T,n}^2 \gg \dots k_{T,1}^2$) whereas BFKL predicts strong ordering in x_i , $x \ll x_n \dots \ll x_1$.

Observe jets at small x in the forward region $Q^2 \simeq k_{T,1}^2 \Rightarrow$ DGLAP evolution suppressed and BFKL evolution left active.

Forward Jets and Single Particle Production

The cross section for forward jet production in DIS was suggested by Mueller (Mueller 1991, Mueller, Navelet 1991) as a means of distinguishing these different **resummation** schemes.



DGLAP and BFKL predict different ordering of the transverse momenta $k_{T,i}$ along the parton cascade developing in DIS jet production. DGLAP predicts strong $k_{T,i}$ ordering ($Q^2 = k_{T,n}^2 \gg \dots k_{T,1}^2$) whereas BFKL predicts strong ordering in x_i , $x \ll x_n \dots \ll x_1$.

Observe jets at small x in the forward region $Q^2 \simeq k_{T,1}^2 \Rightarrow$ DGLAP evolution suppressed and BFKL evolution left active.

Hadronic final state quantities are sensitive to the dynamics of QCD processes and are thus expected to be able to discriminate between different evolution approximations.

Hadronic Final State Quantities

- **Forward Jet Production:**
studied through leading order BFKL and also NLO fixed order ;
various Monte Carlo models (ARIADNE, LEPTO, HERWIG, RAPGAP, LDC) implementing these have been used to compare the data with theoretical predictions. Unfortunately, both BFKL and NLO fixed order QCD calculations can be used to describe the data reasonably well.

Hadronic Final State Quantities

- **Forward Jet Production:**

studied through leading order BFKL and also NLO fixed order ; various Monte Carlo models (ARIADNE, LEPTO, HERWIG, RAPGAP, LDC) implementing these have been used to compare the data with theoretical predictions. Unfortunately, both BFKL and NLO fixed order QCD calculations can be used to describe the data reasonably well.

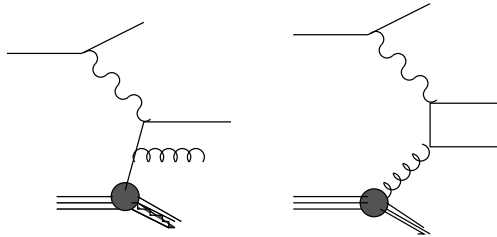
- **Single Particle Production:**

Avoids various uncertainties of forward jet production \Rightarrow jet algorithms, but has been studied only at LO which severely underestimates the data \Rightarrow need to go to NLO to make any definite statements with regard to comparison with data.

NLO calculation of large p_{\perp} hadrons in DIS

The calculation consists of various steps needed to finally define an Infrared Safe Observable.

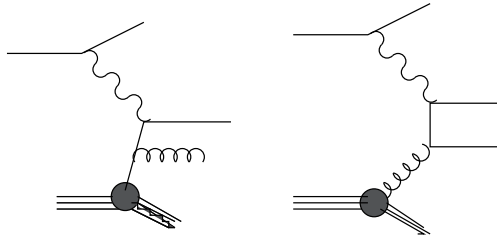
- The Born level partonic cross section $\gamma^* + q \rightarrow g + q$, $\gamma^* + g \rightarrow q + \bar{q}$



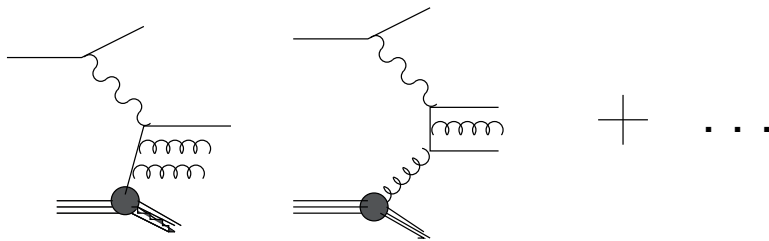
NLO calculation of large p_{\perp} hadrons in DIS

The calculation consists of various steps needed to finally define an Infrared Safe Observable.

- The Born level partonic cross section $\gamma^* + q \rightarrow g + q$, $\gamma^* + g \rightarrow q + \bar{q}$



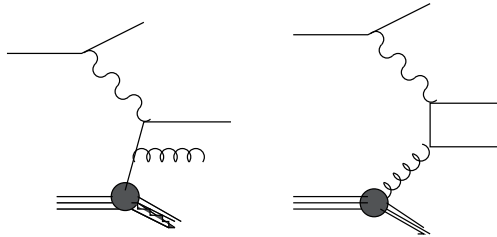
- The Higher Order Correction terms are of the form (real) $\gamma^* + q \rightarrow q + g + g$, $\gamma^* + g \rightarrow q + \bar{q} + g \dots$



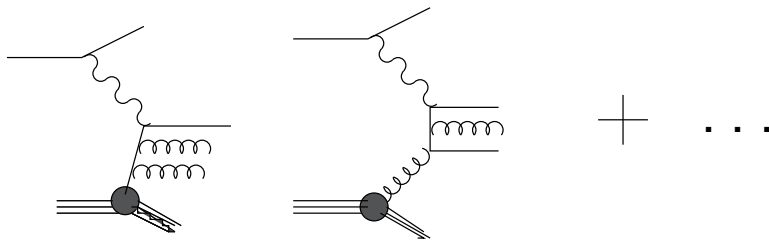
NLO calculation of large p_{\perp} hadrons in DIS

The calculation consists of various steps needed to finally define an Infrared Safe Observable.

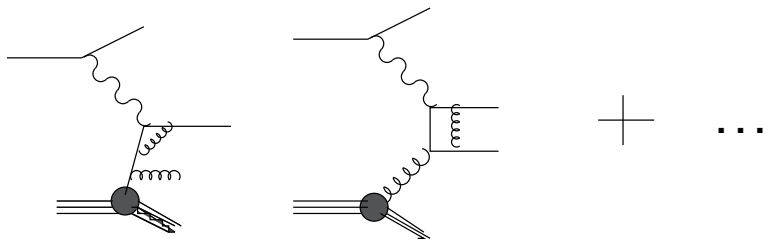
- The Born level partonic cross section $\gamma^* + q \rightarrow g + q$, $\gamma^* + g \rightarrow q + \bar{q}$



- The Higher Order Correction terms are of the form (real) $\gamma^* + q \rightarrow q + g + g$, $\gamma^* + g \rightarrow q + \bar{q} + g \dots$



- And the virtual diagrams



IR problems

- Like all QCD calculations, both real and virtual corrections exhibit infrared singularities which have to be cancelled/absorbed into distribution functions.

IR problems

- Like all QCD calculations, both real and virtual corrections exhibit infrared singularities which have to be cancelled/absorbed into distribution functions.
- For our general $2 \rightarrow 3$ partonic subprocess, virtual and real emission diagrams give various singularities.

IR problems

- Like all QCD calculations, both real and virtual corrections exhibit infrared singularities which have to be cancelled/absorbed into distribution functions.
- For our general $2 \rightarrow 3$ partonic subprocess, virtual and real emission diagrams give various singularities.
- Collinear singularities appear as $\frac{1}{\epsilon}$ divergences in Dim. Reg. Scheme. Infrared (soft) divergences appear at this order as $\frac{1}{\epsilon^2}$

IR problems

- Like all QCD calculations, both real and virtual corrections exhibit infrared singularities which have to be cancelled/absorbed into distribution functions.
- For our general $2 \rightarrow 3$ partonic subprocess, virtual and real emission diagrams give various singularities.
- Collinear singularities appear as $\frac{1}{\epsilon}$ divergences in Dim. Reg. Scheme. Infrared (soft) divergences appear at this order as $\frac{1}{\epsilon^2}$
- $\frac{1}{\epsilon^2}$ pieces cancel when real and virtual diagrams are added. $\frac{1}{\epsilon}$ pieces are absorbed into evolved structure functions (for initial state particles) or evolved fragmentation functions (for final state radiation).

IR problems

- Like all QCD calculations, both real and virtual corrections exhibit infrared singularities which have to be cancelled/absorbed into distribution functions.
- For our general $2 \rightarrow 3$ partonic subprocess, virtual and real emission diagrams give various singularities.
- Collinear singularities appear as $\frac{1}{\epsilon}$ divergences in Dim. Reg. Scheme. Infrared (soft) divergences appear at this order as $\frac{1}{\epsilon^2}$
- $\frac{1}{\epsilon^2}$ pieces cancel when real and virtual diagrams are added. $\frac{1}{\epsilon}$ pieces are absorbed into evolved structure functions (for initial state particles) or evolved fragmentation functions (for final state radiation).
- To carry out this procedure we need a systematic method to extract all these divergences.

General structure of the cross section

Kinematics of the general reaction:

$$e(\ell) + p(P) \rightarrow e(\ell') + h(P_4) + X$$

fixed by momenta of the outgoing lepton and the hadron h (transverse momentum p_{T4} and pseudo rapidity η_4).

$$\frac{d\sigma}{d\varphi dQ^2 dy dE_{\perp 4} d\eta_4} = \frac{\alpha}{2\pi} \sum_{a,b} \int dx G_a(x, M) \int \frac{dz}{z^2} D_b^h(z, M_F) \left\{ \frac{\alpha_s(\mu)}{2\pi} \frac{d\hat{\sigma}_{a,b}^{Born}(x, z)}{d\varphi dQ^2 dy dE_{\perp 4} d\eta_4} + \left(\frac{\alpha_s(\mu)}{2\pi} \right)^2 \frac{dK_{ab}^{HO}(x, z, \mu, M, M_F)}{d\varphi dQ^2 dy dE_{\perp 4} d\eta_4} \right\}$$

$\hat{\sigma}_{a,b}^{Born}(x, z)$ are the subprocess Born cross sections describing the production of a large- p_T parton b and K_{ab}^{HO} are the associated Higher Order corrections.

In actual practise, $\hat{\sigma}_{a,b}^{Born}(x, z)$ and K_{ab}^{HO} are calculated in the virtual photon - proton CMS frame since the H1 collaboration explicitly uses this frame to place cuts on the outgoing hadron transverse momentum.

Regulating IR divergences in our case

A combination of the phase space slicing and subtraction methods is used.

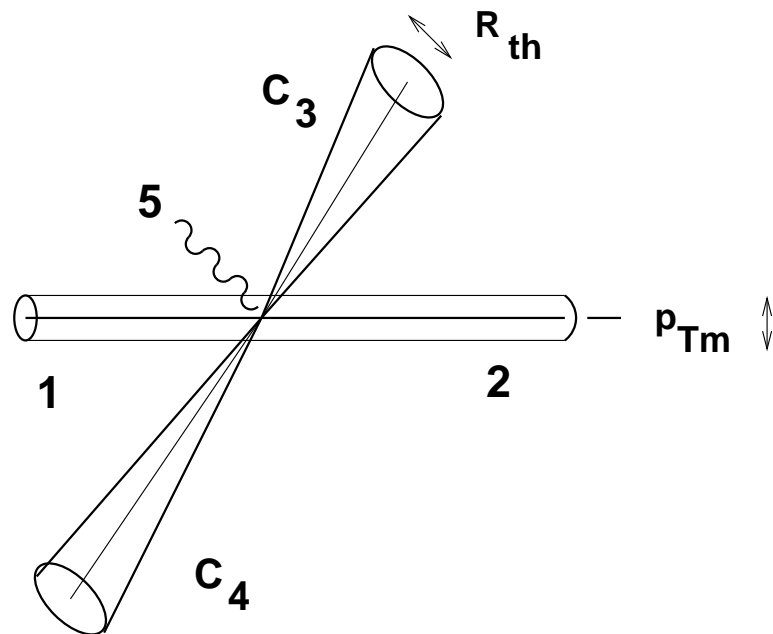
Consider the generic process $1 + 2 \rightarrow 3 + 4 + 5$

Only one of the final state particles can be soft (say **5**) and the others **3** and **4** have a high p_T and are well separated in phase space.

Thus, **5** can be soft, or collinear to any of the four other particles.

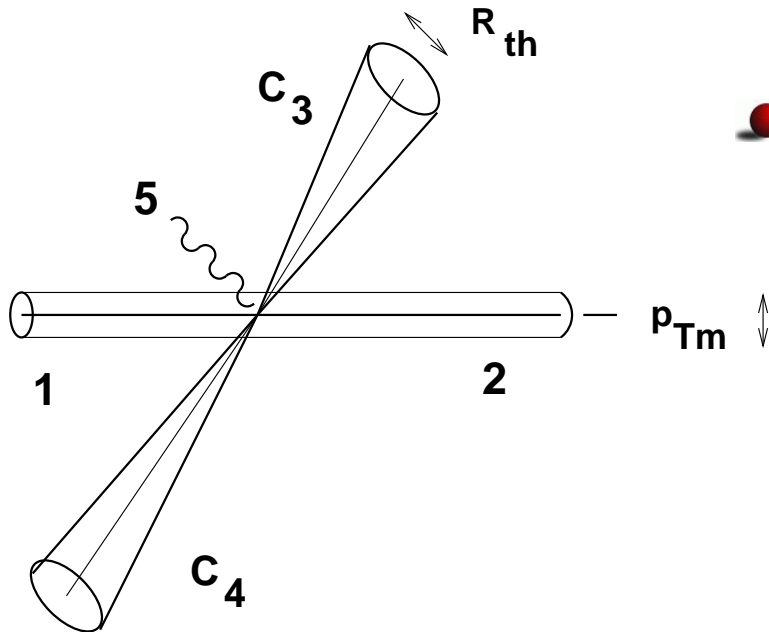
The phase space is now sliced using two arbitrary unphysical parameters p_{Tm} and R_{th}

Regulating IR divergences contd...



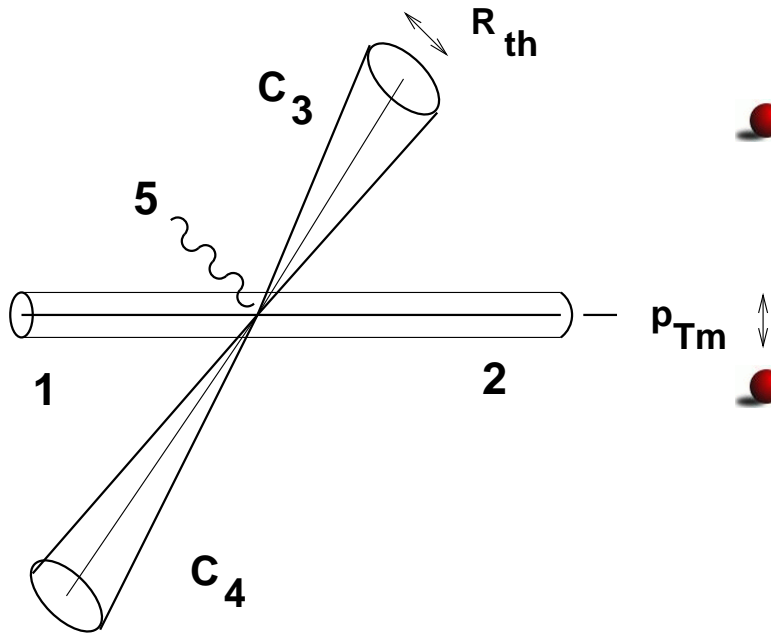
- Part I: $|p_{T5}| < p_{Tm} \ll$ other transverse momenta. This cylinder supplies the IR and initial state collinear singularities (and a small fraction of the final state collinear singularities).

Regulating IR divergences contd...



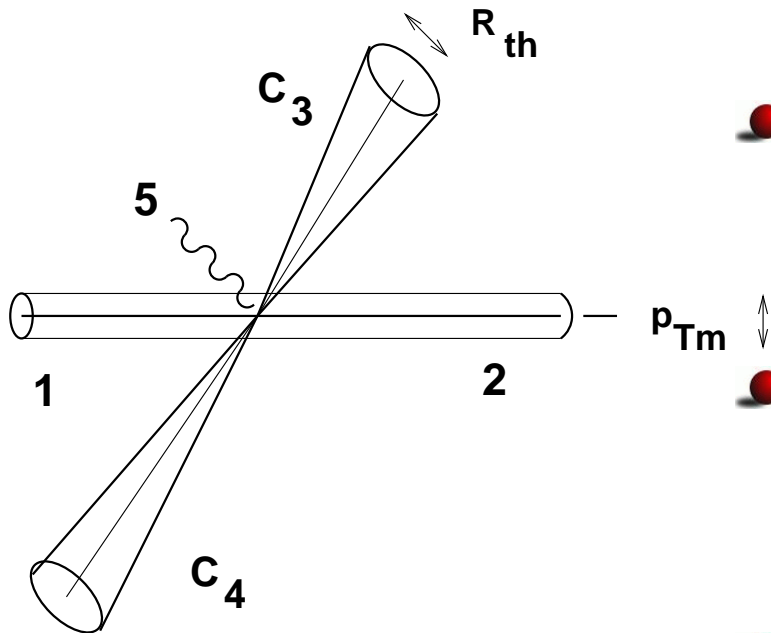
- **Part I:** $|p_{T5}| < p_{Tm} \ll$ other transverse momenta. This cylinder supplies the IR and initial state collinear singularities (and a small fraction of the final state collinear singularities).
- **Part IIa:** $|p_{T5}| > p_{Tm}$ and belongs to a cone C_3 about direction of **3**
 $(y_5 - y_3)^2 + (\phi_5 - \phi_3)^2 \leq R_{th}^2$. C_3 contains the final state collinear singularities for **5//3**

Regulating IR divergences contd...



- **Part I:** $|p_{T5}| < p_{Tm} \ll$ other transverse momenta. This cylinder supplies the IR and initial state collinear singularities (and a small fraction of the final state collinear singularities).
- **Part IIa:** $|p_{T5}| > p_{Tm}$ and belongs to a cone C_3 about direction of **3**
 $(y_5 - y_3)^2 + (\phi_5 - \phi_3)^2 \leq R_{th}^2$. C_3 contains the final state collinear singularities for **5//3**
- **Part IIb:** $|p_{T5}| > p_{Tm}$ and belongs to a cone C_4 about direction of **4**
 $(y_5 - y_4)^2 + (\phi_5 - \phi_4)^2 \leq R_{th}^2$. C_4 contains the final state collinear singularities for **5//4**

Regulating IR divergences contd...



- Part I:** $|p_{T5}| < p_{Tm} \ll$ other transverse momenta. This cylinder supplies the IR and initial state collinear singularities (and a small fraction of the final state collinear singularities).
- Part IIa:** $|p_{T5}| > p_{Tm}$ and belongs to a cone C_3 about direction of **3**
 $(y_5 - y_3)^2 + (\phi_5 - \phi_3)^2 \leq R_{th}^2$. C_3 contains the final state collinear singularities for **5//3**
- Part IIb:** $|p_{T5}| > p_{Tm}$ and belongs to a cone C_4 about direction of **4**
 $(y_5 - y_4)^2 + (\phi_5 - \phi_4)^2 \leq R_{th}^2$. C_4 contains the final state collinear singularities for **5//4**
- Part IIc:** $|p_{T5}| > p_{Tm}$ and belongs to neither of the two cones C_3 or C_4 . This part has no divergence and can be treated directly in 4 dimensions.

IR divergences contd...

- Divergent contributions from regions I, IIa,b are calculated analytically in $d = 4 - 2\epsilon$ and combined with the virtual terms.

IR divergences contd...

- Divergent contributions from regions I, IIa,b are calculated analytically in $d = 4 - 2\epsilon$ and combined with the virtual terms.
- IR divergences cancel, initial (final) state coll. singularities absorbed into parton distribution (fragmentation) functions.

IR divergences contd...

- Divergent contributions from regions I, IIa,b are calculated analytically in $d = 4 - 2\epsilon$ and combined with the virtual terms.
- IR divergences cancel, initial (final) state coll. singularities absorbed into parton distribution (fragmentation) functions.
- Finite remainders of I, IIa,b,c are calculated using a MC integration. These depend on $\ln p_{Tm}$, $\ln^2 p_{Tm}$ for region I and $\ln R_{th}$ for region II a,b.

IR divergences contd...

- Divergent contributions from regions I, IIa,b are calculated analytically in $d = 4 - 2\epsilon$ and combined with the virtual terms.
- IR divergences cancel, initial (final) state coll. singularities absorbed into parton distribution (fragmentation) functions.
- Finite remainders of I, IIa,b,c are calculated using a MC integration. These depend on $\ln p_{Tm}$, $\ln^2 p_{Tm}$ for region I and $\ln R_{th}$ for region II a,b.
- Terms proportional to p_{Tm} and R_{th} are dropped (small). The log terms cancel when all the parts are combined (p_{Tm} and R_{th} are chosen small but not too small to prevent numerical instabilities).

The results in this talk are based on the following:

- P. Aurenche, RB, M. Fontannaz and R. M. Godbole, Eur. Phys. J. C **34**, 277 (2004) [arXiv:hep-ph/0312359] (NLO Direct + LO Resolved)
- P. Aurenche, RB, M. Fontannaz and R. M. Godbole, Eur. Phys. J. C **42**, 43 (2005) [arXiv:hep-ph/0504008] (NLO Direct + NLO Resolved (resummed))
- P. Aurenche, R. Basu and M. Fontannaz, arXiv:0807.2133 [hep-ph]. (to appear in EPJC)

Results

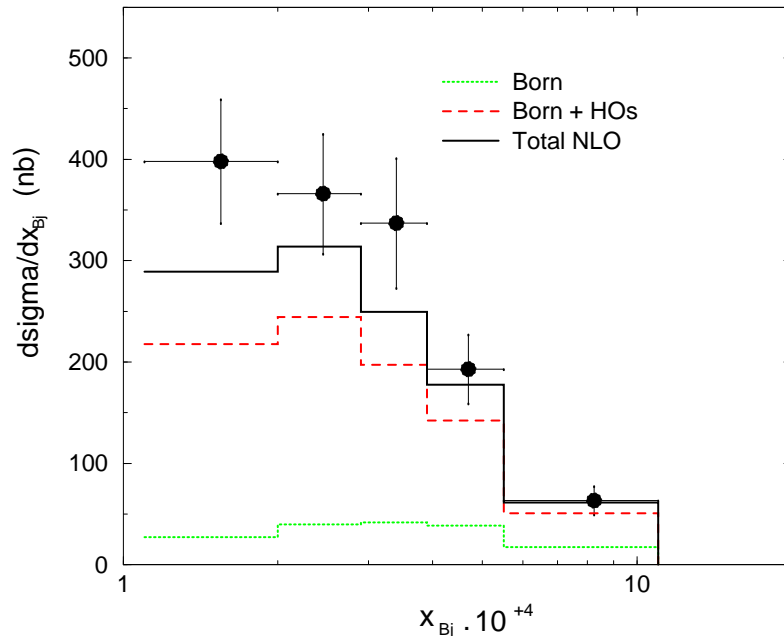
$$4.5 \text{ GeV}^2 \leq Q^2 \leq 15 \text{ GeV}^2$$

$$p_T^* > 2.5 \text{ GeV}$$

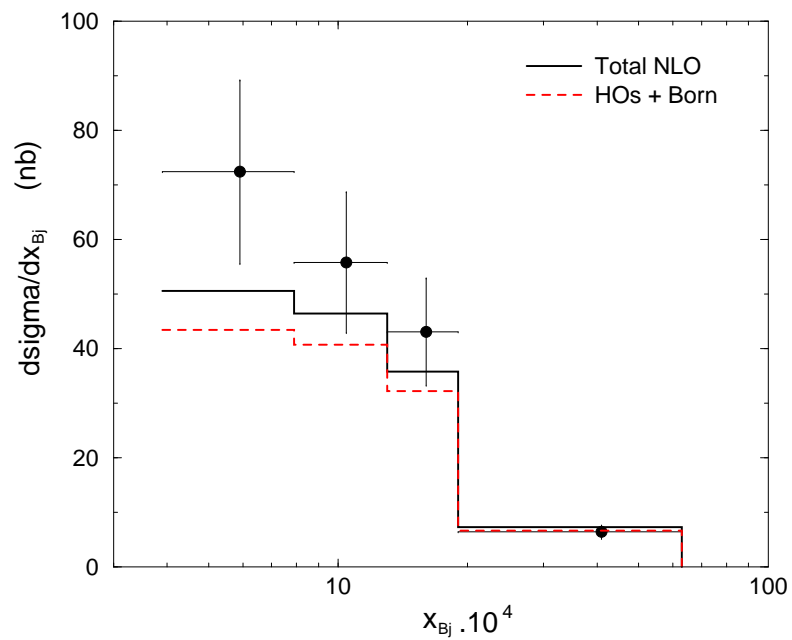
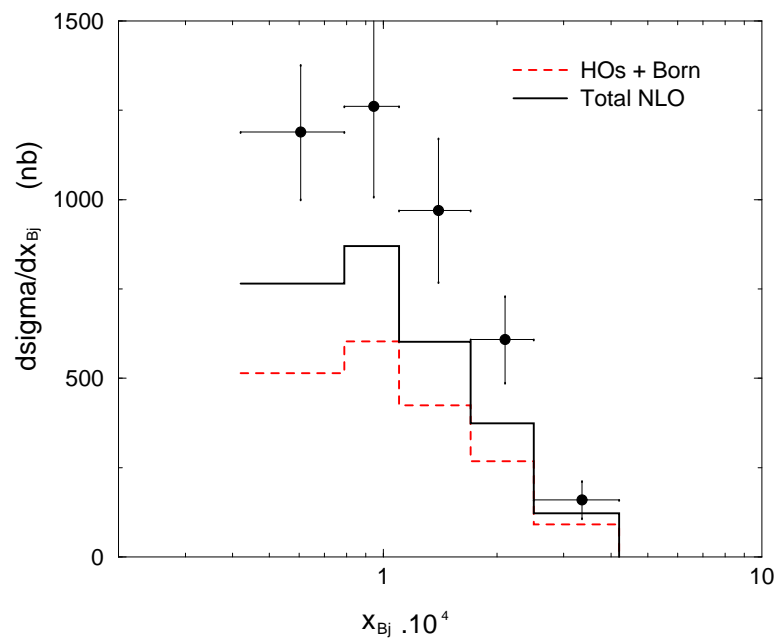
$$.1 < y < .6$$

$$5^\circ \leq \theta_\pi^{Lab} \leq 25^\circ$$

$$x_\pi = E_\pi^{Lab} / E_{proton}^{Lab} \geq .01$$



Size of the HO corrections is large, particularly at low x_{Bj} . HO_s corresponds to HO contributions from where the resolved contribution has been subtracted out. (will return to this later)



Data and results for $2 < Q^2 < 4.5 \text{ GeV}^2$ and $15 < Q^2 < 70 \text{ GeV}^2$ Note that the resolved component decreases when Q^2 increases as also when x_{Bj} increases.

Resolved Photon contribution

HO correction \Rightarrow contribution proportional to $\ln \frac{E_{\perp 4}^2}{Q^2}$ when $E_{\perp 4}^2 \gg Q^2 \Rightarrow$ integration over $E_{\perp 5}$ - the unobserved final quark momentum \Rightarrow configuration in which the final quark is collinear to the virtual photon. In fact, for the $2 \rightarrow 2$ process

$$\sigma_{\perp} \simeq \int dz P_{q\gamma}(z) \left\{ \log \frac{E_{\perp 4}^2}{Q^2} \right\} \hat{\sigma}(0) dps$$

with $P_{q\gamma}(z) = \frac{\alpha}{2\pi} (z^2 + (1-z)^2)$ and the quark distribution in the virtual photon

$$q_{\gamma}(z, E_{\perp 4}, Q^2) = P_{q\gamma}(z) \log \frac{E_{\perp 4}^2}{Q^2}$$

Resolved Photon Contribution \Rightarrow calculated in the pure QED limit. When $E_{\perp 4}^2 \gg Q^2$ need to include LO or NLO QCD corrections (because terms like $\alpha_s \ln \frac{E_{\perp 4}^2}{Q^2}$ appear. However in the kinematical configuration of the H1 experiment, this lowest order expression is sufficient. The **resolved photon** contribution dies out with increasing virtuality of the photon and goes as

$$\sigma_{\perp} \simeq \int dz P_{q\gamma}(z) \left\{ \log \frac{E_{\perp 4}^2 + Q^2}{Q^2} \right\} \hat{\sigma}(0) dps$$

Results contd...

- Theory underestimates data by a small amount

Results contd...

- Theory underestimates data by a small amount
- We need to consider the scale dependence of the results (which here have been calculated at

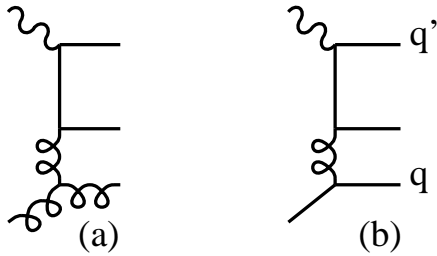
$$\mu = M = M_F = (Q^2 + E_{\perp 4}^2)^{1/2}$$

Results contd...

- Theory underestimates data by a small amount
- We need to consider the scale dependence of the results (which here have been calculated at $\mu = M = M_F = (Q^2 + E_{\perp 4}^2)^{1/2}$)
- We need to look at the HO corrections to the resolved part which are large - this when included gives $HO/Born \simeq 1$ in the kinematical domain of the graphs shown

Some details of the HO corrections

- The two largest contributions come from

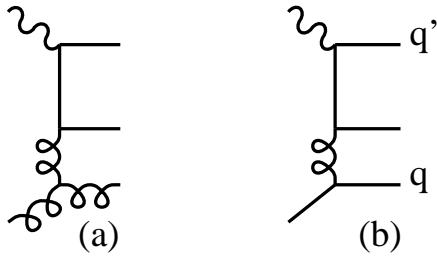


⇒ exchange of a gluon in the t-channel.

- **These are qualitatively new subprocesses not present at the Born level** *i.e.* they do not possess singular configurations of partons which contribute to the dressing up of the distribution (fragmentation) functions already present in the Born term.

Some details of the HO corrections

- The two largest contributions come from

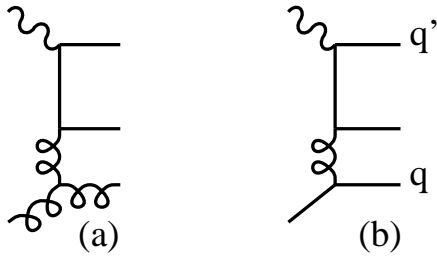


⇒ exchange of a gluon in the t-channel.

- **These are qualitatively new subprocesses not present at the Born level** *i.e.* they do not possess singular configurations of partons which contribute to the dressing up of the distribution (fragmentation) functions already present in the Born term.
- ⇒ These graphs (with a trigger on the g or q but *not* on q') are the lowest order BFKL terms in which extra gluons are emitted by the t-channel gluon

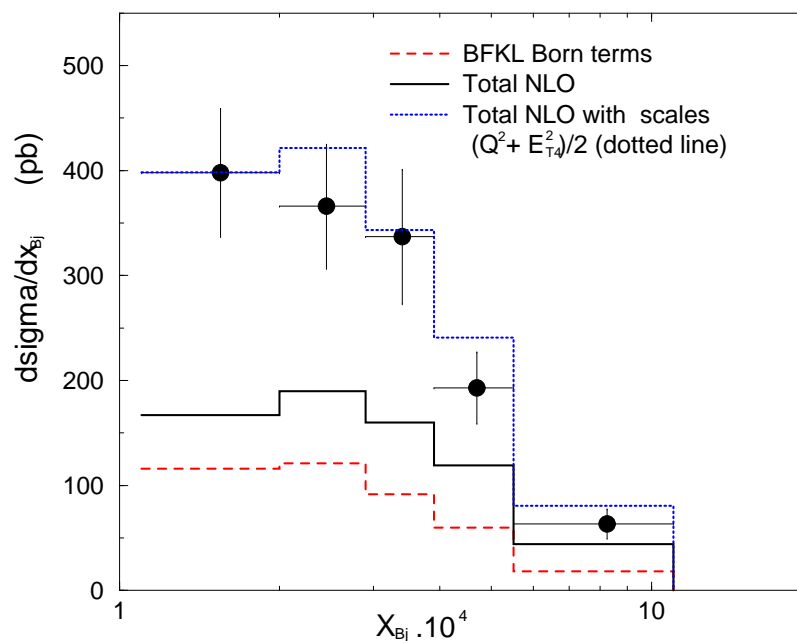
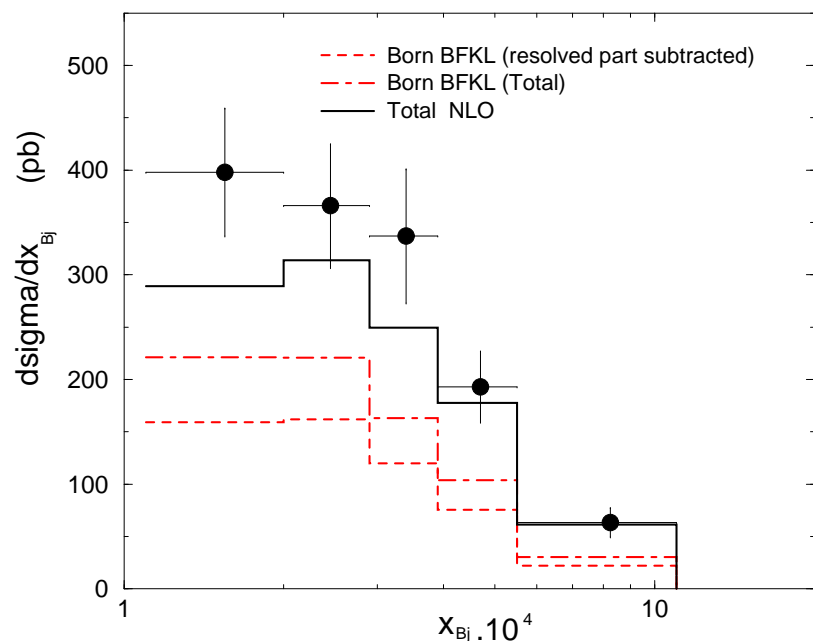
Some details of the HO corrections

- The two largest contributions come from



⇒ exchange of a gluon in the t-channel.

- **These are qualitatively new subprocesses not present at the Born level** *i.e.* they do not possess singular configurations of partons which contribute to the dressing up of the distribution (fragmentation) functions already present in the Born term.
- ⇒ These graphs (with a trigger on the g or q but *not* on q') are the lowest order BFKL terms in which extra gluons are emitted by the t-channel gluon
- These therefore contribute precisely to the **forward cross section** that HERA experiments are supposed to study to reveal BFKL dynamics

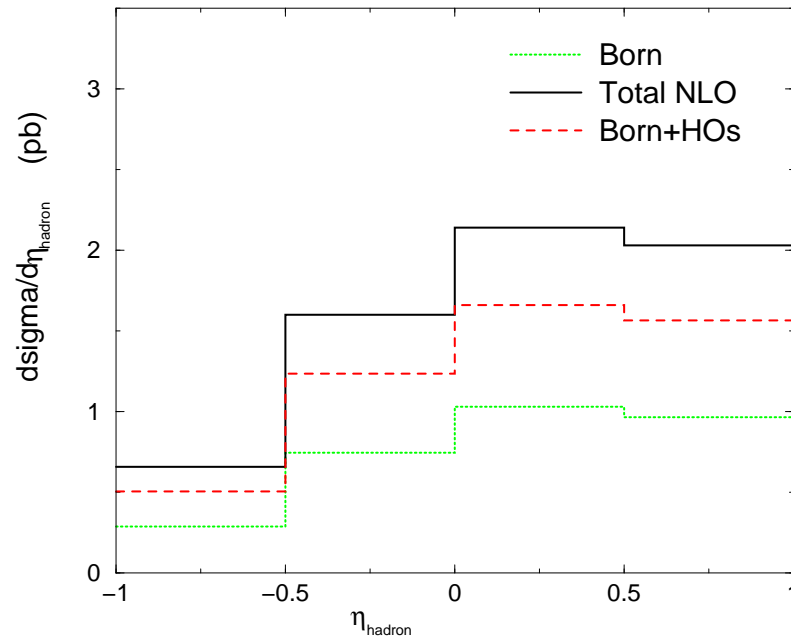
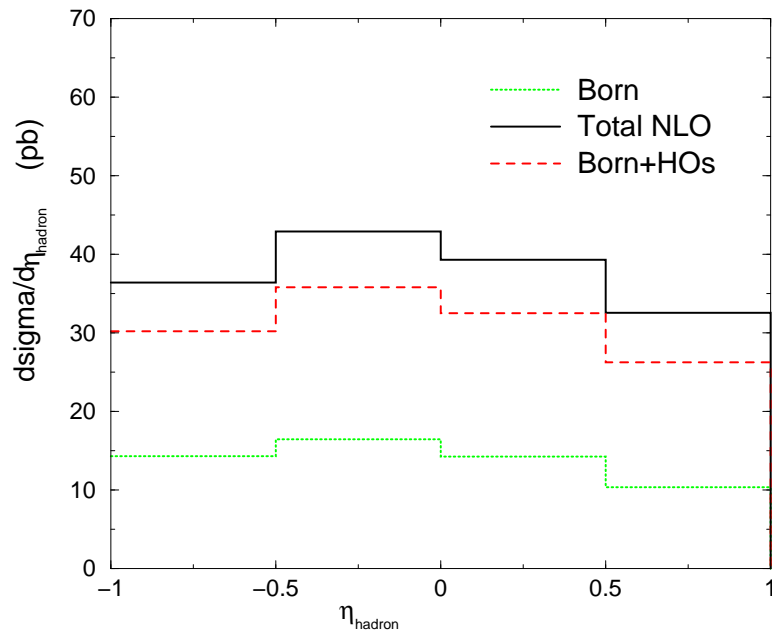


The BFKL Born contribution is more than **two thirds of the total NLO correction**.

⇒ Main part of the forward cross section is due to the BFKL Born terms ($\gamma^* q \rightarrow q' \bar{q}' q$ and $\gamma^* q \rightarrow q \bar{q} g$).

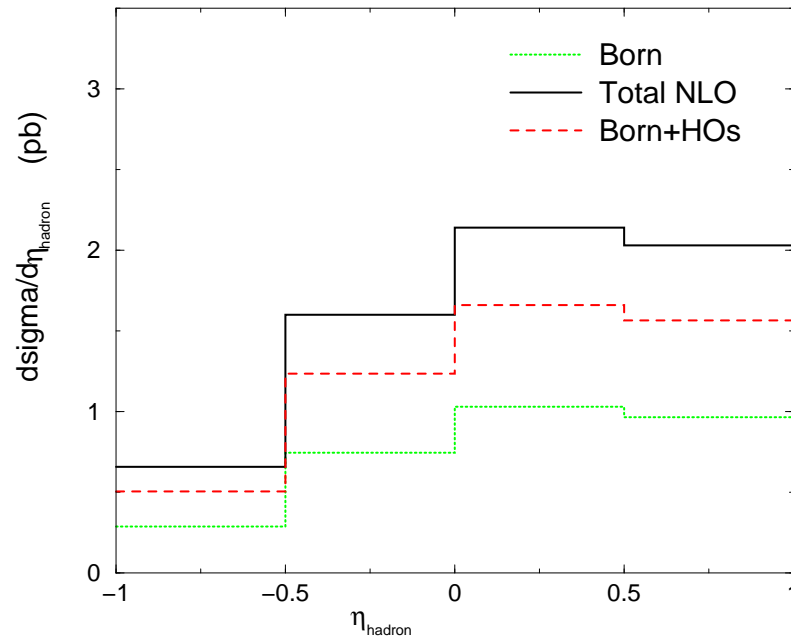
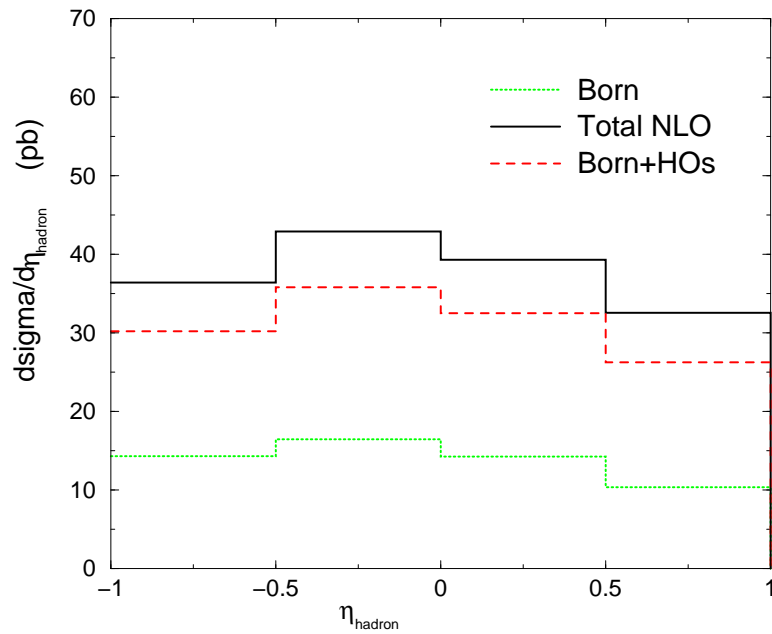
⇒ these channels are therefore strongly dependent on renormalization and factorization scales.

⇒ There is room for a BFKL-ladder contribution between data and present theoretical predictions if scale $M \sim p_T^{parton}$ but not with the more realistic $M \sim p_T^{hadron}$



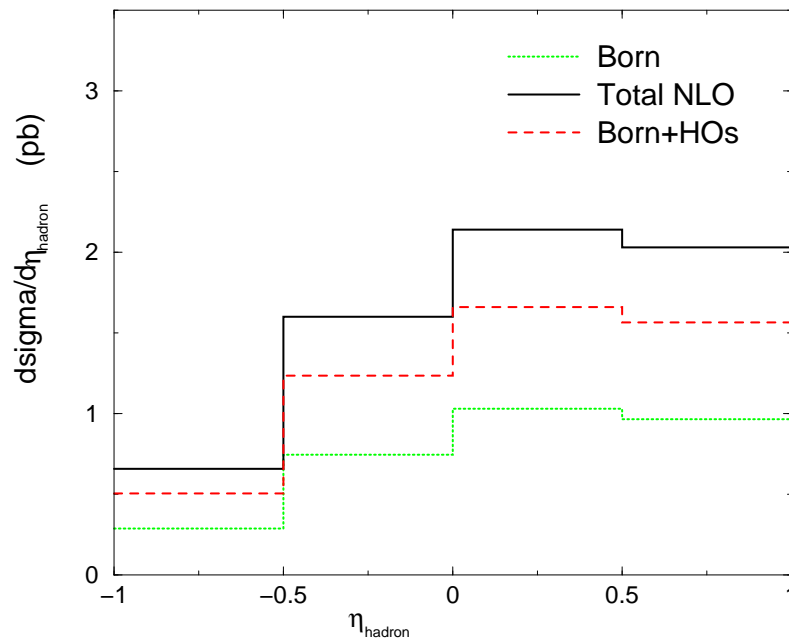
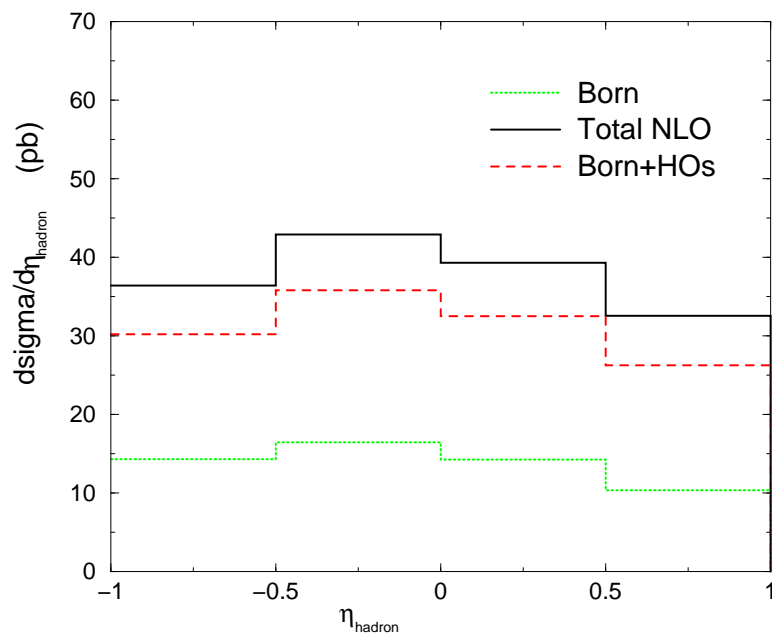
$d\sigma/d\eta_{hadron}$ large- E_{\perp} π^0 cross section integrated over E_{\perp} with cuts $E_{\perp} > 3$ GeV and $E_{\perp} > 7$ GeV. $\sqrt{S_{ep}} = 300$ GeV, $.3 \leq y \leq .7$ and $-1 \leq \eta_{hadron} \leq 1$:
 $5 \text{ GeV}^2 \leq Q^2 \leq 10 \text{ GeV}^2$

● The ratio $r = \frac{HO_s}{Born}$ decreases as the cut on E_{\perp} increases



$d\sigma/d\eta_{hadron}$ large- E_{\perp} π^0 cross section integrated over E_{\perp} with cuts $E_{\perp} > 3$ GeV and $E_{\perp} > 7$ GeV. $\sqrt{S_{ep}} = 300$ GeV, $.3 \leq y \leq .7$ and $-1 \leq \eta_{hadron} \leq 1$:
 $5 \text{ GeV}^2 \leq Q^2 \leq 10 \text{ GeV}^2$

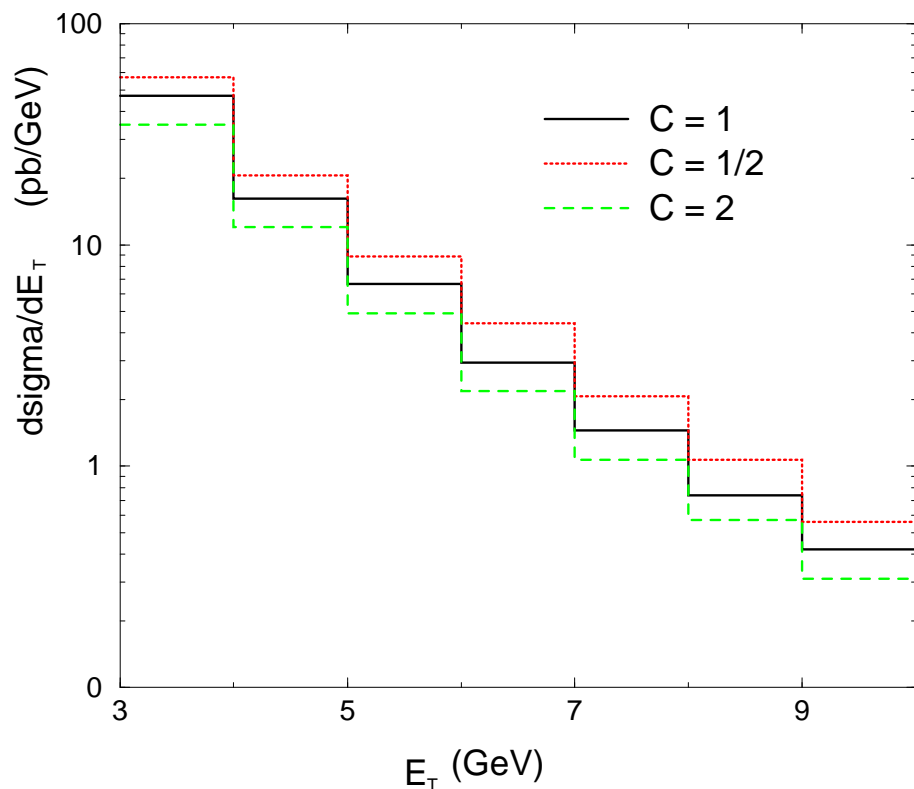
- The ratio $r = \frac{HO_s}{Born}$ decreases as the cut on E_{\perp} increases
- The ratio of the resolved contribution to the Born *increases* as cut on E_{\perp} increases \Rightarrow because of larger value of $(Q^2 + E_{\perp}^2)/Q^2$



$d\sigma/d\eta_{hadron}$ large- E_{\perp} π^0 cross section integrated over E_{\perp} with cuts $E_{\perp} > 3$ GeV and $E_{\perp} > 7$ GeV. $\sqrt{S_{ep}} = 300$ GeV, $.3 \leq y \leq .7$ and $-1 \leq \eta_{hadron} \leq 1$:
 $5 \text{ GeV}^2 \leq Q^2 \leq 10 \text{ GeV}^2$

- The ratio $r = \frac{HO_s}{Born}$ decreases as the cut on E_{\perp} increases
- The ratio of the resolved contribution to the Born *increases* as cut on E_{\perp} increases \Rightarrow because of larger value of $(Q^2 + E_{\perp}^2)/Q^2$
- In photoproduction, this ratio is much larger. since the virtuality of the photon suppresses the resolved contribution

Scale dependence of the cross section



We use scales $\mu = M = M_F = C\sqrt{Q^2 + E_{\perp}^2}$ with $C = \frac{1}{2}, 1, 2..$

A change of scales by a factor 4 results in a change of cross section by a factor 2 \Rightarrow even at large E_{\perp} cross section very sensitive to scales.

Higher Order Resolved

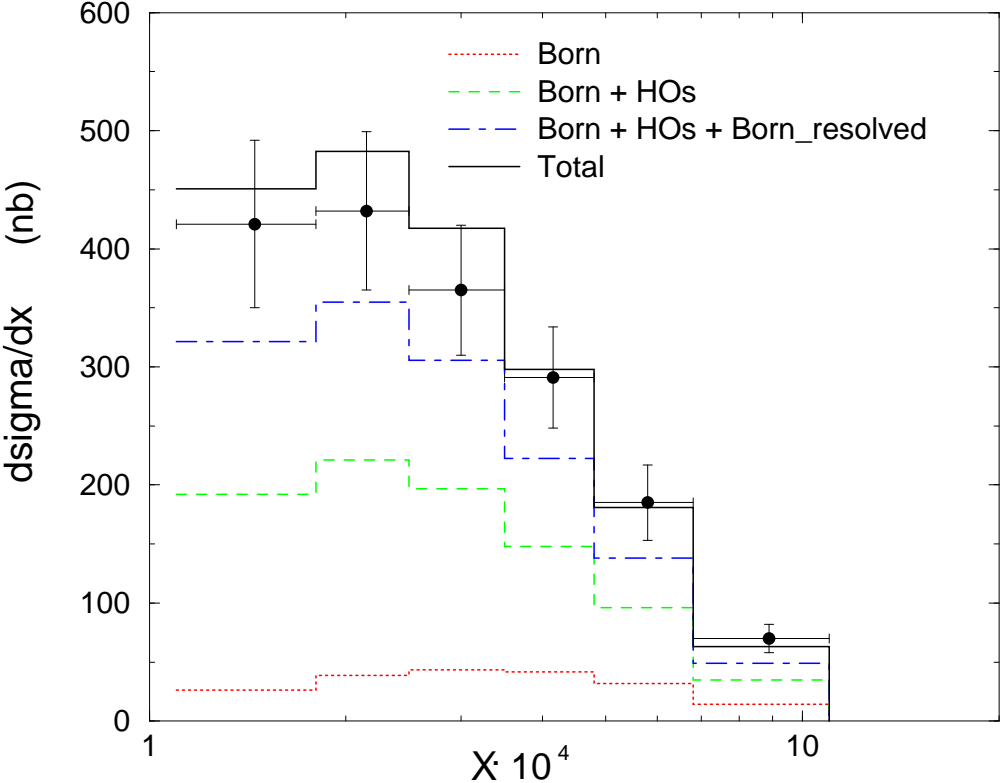
All these results were obtained with NLO direct but LO resolved.

Fine when E_{\perp}^2 is close to Q^2 but not for E_{\perp}^2 large.

However including the HO resolved contributions (Fontannaz) changes the situation.

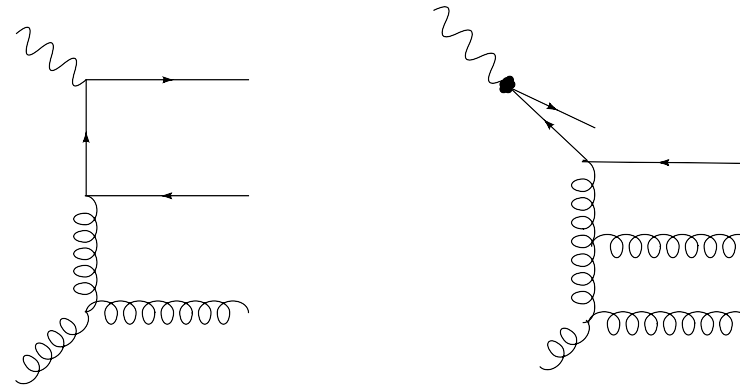
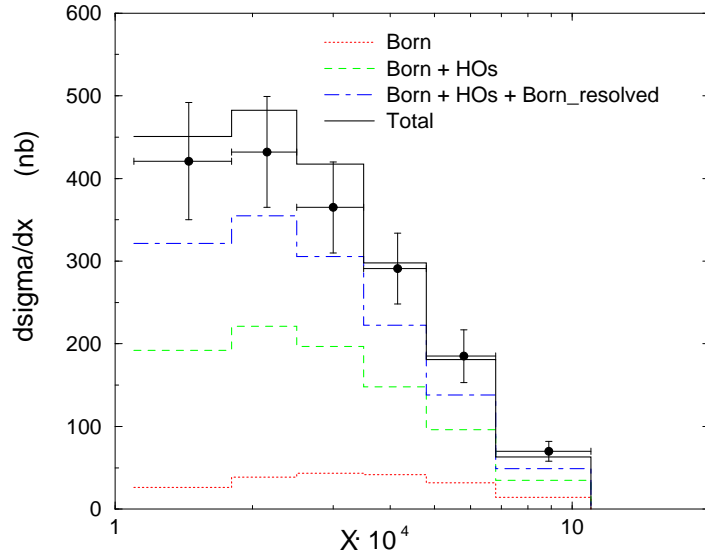
- HO corrections to the direct term are large (due to gluon in the t channel)
- NLO direct term depends strongly on renormalisation scale
- The NLO resolved contribution is as large as the NLO direct at factorisation scale
$$M_{\gamma}^2 = Q^2 + E_{\perp}^2$$
- With the "natural" scale $Q^2 + E_{\perp}^2$ total cross section is in good agreement with H1 \Rightarrow sizable BFKL contribution may not be necessary.
- Scale dependence is substantially reduced (detailed study is possible to compare various differential cross sections with H1 predictions – done in paper 2).

Results



Azimuthal Correlations

Main summary of our result from the previous work:



- Small Born term, higher order term large, because of the presence of the gluon pole
- The resolved contribution is also large for the same reason, the LO and NLO being similar to $p\bar{p}$ except for proton PDF being replaced by photon PDF (which are less steep).
- The two diagrams can be seen as the lowest order terms of the BFKL ladder between the photon (backward direction) and the proton (forward direction).

Azimuthal Correlations

- If the available phase space (rapidity) is large between the forward and backward partons \Rightarrow expect multiple gluon emission \Rightarrow expect BFKL dynamics to dominate
- If not, then at most one or two-gluon emission is appropriate

The good agreement between our earlier work and H1 seems to favour the latter

\Rightarrow test using forward hadron-jet azimuthal correlations

Forward Hadron-jet azimuthal correlations

- Rapidity dependence of cross section
- $\cos(\pi - \phi)$

Hadronic CM frame: $0.1 \leq y \leq 0.7$, $1 \leq 10^4 x_{Bj} \leq 5$,

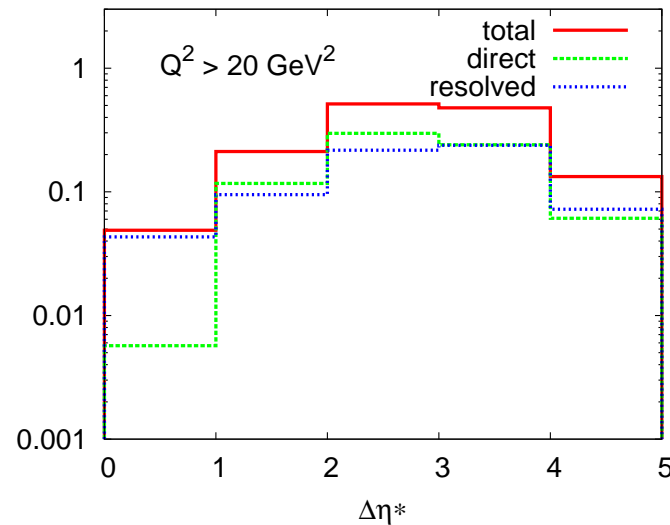
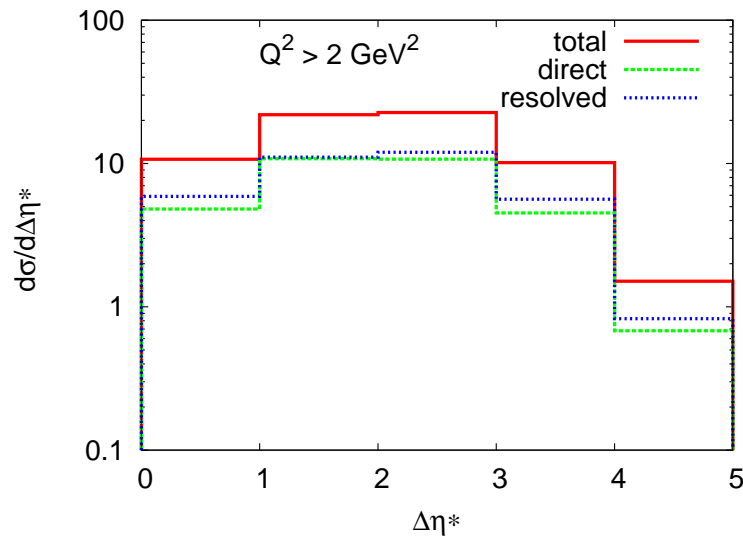
Forward pion: $5^\circ \leq \theta_\pi^{lab} \leq 25^\circ$; $.01 \leq x_\pi = E_\pi^{lab} / E_p^{lab} \leq 1$.

$Q^2 \leq 50 \text{ GeV}^2$, $p_\perp^{*\pi} \geq 4 \text{ GeV}$; $p_\perp^{*jet} \geq 3.5 \text{ GeV}$

The last cut avoids too large HO corrections in some regions of phase space.

Cross section vs rapidity gap

Variation of the cross section as a function of the rapidity gap between the forward pion and the largest p_{\perp} jet



- No rapidity plateau, maximum moves to larger values of the $\Delta\eta$ as Q_{min}^2 and hence y increases
- The resolved contribution is flatter than the direct because it involves an extra convolution with the parton distribution function in the photon

Cross section vs rapidity gap

$$y = \frac{p_{\perp}^*}{\sqrt{S}} \frac{2P}{\sqrt{S}} (e^{-y_1} + e^{-y_2})$$

$$x_1 = \frac{p_{\perp}^*}{\sqrt{S}} \frac{\sqrt{S}}{2P} (e^{y_1} + e^{y_2}) + x_{Bj}$$

(x_1 is fraction of the proton momentum carried by the struck quark)

⇒ variation in x_1 and y in terms of final state rapidities ⇒ dependence of the PDF's of P and γ on the final state rapidities.

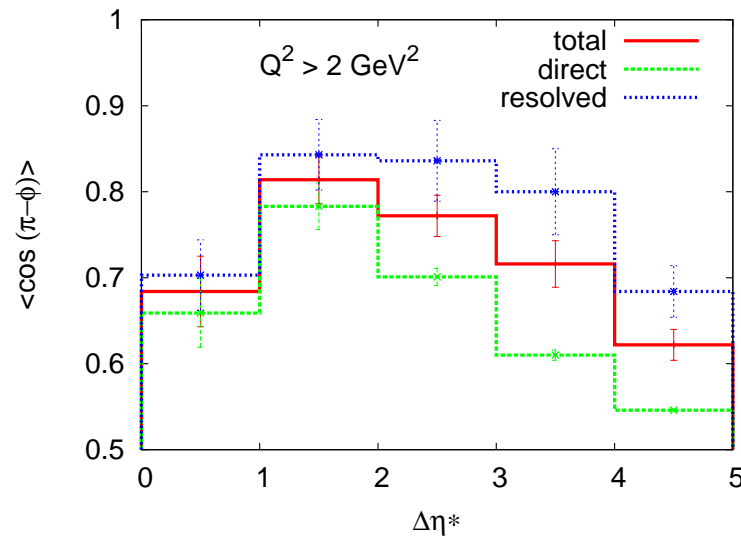
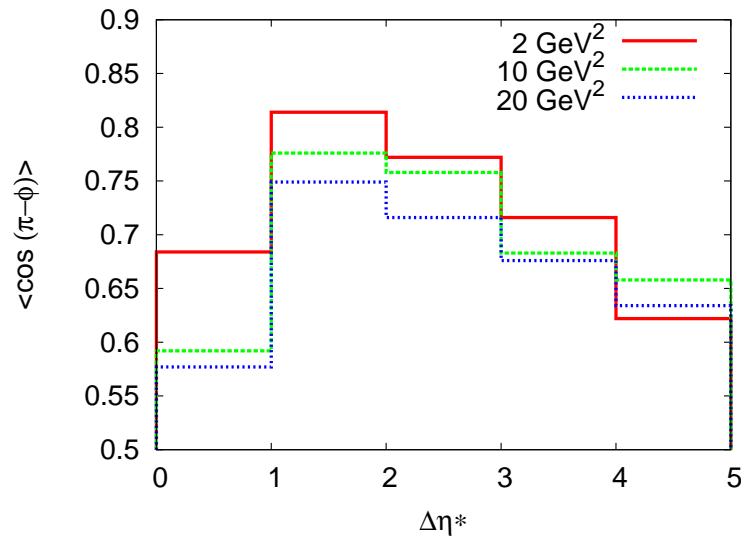
- second forward parton gives larger x_1 , backward parton gives larger y .
- these kinematical domains are suppressed by the large x_1 and large y behaviour of the respective PDF's.

The extra convolution of the resolved case flattens the distribution (and also moves it to the right)

(The H1 result is for a dijet cross section vs rapidity and also forward jet and dijet system cross section with small rapidity separation)

We have also similar results for forward pion and jet with largest rapidity gap with the pion.

$\langle \cos(\pi - \phi) \rangle$ vs rapidity gap



- $\langle \cos(\pi - \phi) \rangle$ decreases as $\Delta\eta^*$ increases \Leftarrow increase of phase space available for the $2 \rightarrow 3$ subprocess.
- Direct component has much faster decorrelation as $\Delta\eta^*$ increases because of rapid growth of the HO component.
- $\langle \cos(\pi - \phi) \rangle$ decreases as Q_{min}^2 increases \Leftarrow the $2 \rightarrow 3$ subprocess becoming more isotropic.
- Dip in the graph for small $\Delta\eta^* \rightarrow$????

NLO vs. BFKL?

Behaviour of $\langle \cos(\pi - \phi) \rangle$ vs. $\Delta\eta^*$ strongly dependent on kinematical constraints \Rightarrow exactly respected in our NLO calculation and has strong effect near $\Delta\eta^* \sim 0$.



The fact that usual BFKL does not respect total energy conservation implies that it will give quite different predictions.